JOURNAL OF GEOPHYSICAL RESEARCH, VOL. 111, D16206, doi:10.1029/2005JD006717, 2006

Interactive dust-radiation modeling: A step to improve weather forecasts

Carlos Pérez,[1] Slobodan Nickovic,[2,3] Goran Pejanovic,[4] José María Baldasano,[1] and Emin Özsoy[5]

Received 27 September 2005; revised 6 March 2006; accepted 5 May 2006; published 25 August 2006.

[1] Inclusion of mineral dust radiative effects could lead to a significant improvement in the radiation balance of numerical weather prediction models with subsequent improvements in the weather forecast itself. In this study the radiative effects of mineral dust have been fully incorporated into a regional atmospheric dust model. Dust affects the radiative fluxes at the surface and the top of the atmosphere and the temperature profiles at every model time step when the radiation module is processed. These changes influence the atmospheric dynamics, moisture physics, and near-surface conditions. Furthermore, dust emission is modified by changes in friction velocity and turbulent exchange coefficients; dust turbulent mixing, transport, and deposition are altered by changes in atmospheric stability, precipitation conditions, and free-atmosphere winds. A major dust outbreak with dust optical depths reaching 3.5 at 550 nm over the Mediterranean region on April 2002 is selected to assess the radiative dust effects on the atmosphere at a regional level. A strong dust negative feedback upon dust emission (35–45% reduction of the AOD) resulted from the smaller outgoing sensible turbulent heat flux decreasing the turbulent momentum transfer from the atmosphere and consequently dust emission. Significant improvements of the atmospheric temperature and mean sea-level pressure forecasts are obtained over dust-affected areas by considerably reducing both warm and cold temperature biases existing in the model without dust-radiation interactions. This study demonstrates that the use of the proposed model with integrated dust and atmospheric radiation represents a promising approach for further improvements in numerical weather prediction practice and radiative impact assessment over dust-affected areas.

Citation: Pérez, C., S. Nickovic, G. Pejanovic, J. M. Baldasano, and E. Özsoy (2006), Interactive dust-radiation modeling: A step to improve weather forecasts, *J. Geophys. Res.*, *111*, D16206, doi:10.1029/2005JD006717.

1. Introduction

[2] Mineral dust particles affect the atmospheric radiation budget through absorption and scattering of incoming solar radiation, and absorption and reemission of outgoing long-wave radiation. The *Intergovernmental Panel on Climate Change* (*IPCC*) [2001] has identified mineral dust as the aerosol with major uncertainty in the climate system. Both the magnitude and the sign of the dust direct radiative forcing remain unresolved and depend on the optical properties of dust, its vertical distribution, cloud cover, and albedo of the underlying surface. The major direct forcing uncertainties are related to the degree of absorbed solar radiation [*Sokolik and Toon*, 1999], the influence on long-wave radiation and the global amount of dust in the atmosphere.

[3] Other uncertainties relate to the effect of dust on cloud formation and precipitation. Concerning the indirect effect (microphysical cloud-dust interactions), *Rosenfeld et al.* [2001] observed that mineral dust generates large concentrations of cloud condensation nuclei (CCN), mostly in the small size range that can lead to cloud formation dominated by small droplets. As a result, this could lead to droplet coalescence reduction and suppressed precipitation. *Levin et al.* [1996] on the other hand found out that mineral dust coated with sulfate and other soluble materials can generate large CCN and consequently large drops, which would accelerate precipitation development through a droplet growth by collection. Additionally, by the so-called "semi-direct" effect dust affecting the thermal atmospheric structure can modify cloud formation [*Hansen et al.*, 1997].

[4] Many studies have explored the radiative forcing of mineral dust [e.g., *Tegen and Lacis*, 1996; *Sokolik and Toon*, 1996; *Quijano et al.*, 2000; *Woodward*, 2001; *Myhre et al.*, 2003] with a wide range of results. *Miller and Tegen* [1998] examined the radiative effect in a climate model by using

[1]Barcelona Supercomputing Center, Earth Sciences Division, Barcelona, Spain.
[2]Euro-Mediterranean Center on Insular Coastal Dynamics, Foundation for International Studies, University of Malta, Valletta, Malta.
[3]Now at Environment Division, Atmospheric Research and Environment Program, World Meteorological Organization, Geneva, Switzerland.
[4]South Environment and Weather Agency (SEWA), Belgrade, Serbia.
[5]Institute of Marine Sciences, Middle East Technical University, Erdemli-Mersin, Turkey.

0148-0227/06/2005JD006717$09.00

prescribed dust distributions. In spite of simplified dust representation in this study, dust and atmosphere generated complex interactions: the increased dust load modified the thermal and dynamic structure of the air and the modified atmosphere furthermore changed dust emission, transport and deposition. More recently, *Perlwitz et al.* [2001] and *Miller et al.* [2004a, 2004b] interactively coupled a dust aerosol model and a general circulation model (GCM).

[5] Several other studies suggest that the inclusion of mineral dust radiative effects would improve the radiation balance of numerical weather prediction (NWP) models and thus increase overall accuracy of the weather prediction itself [*Kischa et al.*, 2003; *Haywood et al.*, 2005].

[6] Most of current weather forecasting models use prespecified (climatological or other) ozone and CO_2 profiles in radiation calculations. Concerning the mineral aerosol and its impact on radiation, current situation is rather unsatisfactory. To our knowledge, none of the operational atmospheric models uses online predicted mineral aerosol concentration for radiation calculations. For example, the NCEP regional models (Eta and NMM) use the solar constant reduced by 3% anywhere anytime to represent aerosol influence. Advances in dust modeling over the last decade have achieved today a level permitting rather accurate dust concentration inputs for calculating dust-radiation interactions. For example, the DREAM dust operational model [*Nickovic et al.*, 2001] is capable of predicting major dust events with considerable accuracy [*Yin et al.*, 2005; *Pérez et al.*, 2006].

[7] Following the idea of improving weather forecasts by including the dust radiative effect, we have completed and refined some preliminary studies [*Nickovic et al.*, 2004; *Nickovic*, 2005]. A parameterization scheme that considers dust aerosol as a radiatively active substance interacting with short- and long-wave radiation has been developed. The modeling system uses the limited-area NCEP/Eta model as an atmospheric driver of the DREAM model. The developed parameterization scheme that integrates these two model components permits two-way interactions between dust and the atmosphere. Within every model time step both dust and atmospheric fields are updated through their mutual influences.

[8] The paper is structured as follows: in section 2 we describe the DREAM modeling system and the new developments introduced. Two simulations of a major dust outbreak that occurred in the Mediterranean region on April 2002 are performed. In the first experiment dust is considered as a dynamic tracer without any radiative interaction. In the other experiment, interaction between short- and long-wave radiation and dust is included. In section 3 we explore the dust direct radiative effects on solar and terrestrial wavelengths, the changes produced on surface turbulent fluxes and the feedback upon dust emission. In this section we also evaluate the forecasted atmospheric temperature and mean sea level pressure from both experiments against objective analysis.

2. Methodology

2.1. Dust Regional Atmospheric Modeling System (DREAM)

[9] DREAM (see *Nickovic et al.* [2001] for details) is a model designed to simulate and/or predict the atmospheric cycle of mineral dust aerosol. It solves the Euler-type partial differential nonlinear equation for dust mass continuity. DREAM is fully embedded as one of the governing prognostic equations in the atmospheric NCEP/Eta atmospheric model [*Janjic*, 1977, 1979, 1984, 1990, 1994, 1996a, 1996b; *Mesinger et al.*, 1988; *Zhao and Carr*, 1997]. The concentration equation simulates all major processes of the atmospheric dust cycle. During the model integration, calculation of the surface dust injection fluxes is made over the model cells declared as deserts. Once injected into the air, dust aerosol is driven by the atmospheric model variables: by turbulence in the early stage of the process when dust is lifted from the ground to the upper levels; by winds in the later phases of the process when dust travels away from the sources; and finally, by thermodynamic processes and rainfall of the atmospheric model and land cover features which provide wet and dry deposition of dust over the Earth surface.

[10] One of the key components of the dust model is the treatment of sourcing terms in the dust concentration continuity equation. Failure to adequately simulate/predict the production phase of the dust cycle leads to wrong representation of all other dust processes in the model. Therefore special attention is made to properly parameterize the dust production phase. Wind erosion of the soil in DREAM parameterization scheme is controlled mainly by type of soil, type of vegetation cover, soil moisture content, and surface atmospheric turbulence. The major input data used to distinct the dust productive soils from the others are a global data set on land cover. Another data participating in dust production calculations is a global soil texture data set from which particle size parameters are evaluated. DREAM has been delivering operational dust forecasts over the Mediterranean region in the last years (currently at http://www.bsc.es/projects/earthscience/DREAM/) and over east Asia. In the operational version, for each texture class fraction four particle size classes (clay, small silt, large silt, and sand) are estimated with particle size radii of 0.73, 6.1, 18, and 38 μm, respectively. For the synoptic-scale transport, only the first two dust classes are relevant for the analysis since their lifetime is larger than about 12 hours.

2.2. New Model Developments

[11] In the new model version, dust is treated as a radiatively active substance interacting with both short and long-wave radiation. Within every model time step both aerosol and atmospheric fields are updated due to their mutual influences.

[12] In order to couple dust and radiation processes, a radiative transfer model including aerosol effects developed at the Goddard Climate and Radiation Branch has been implemented into the NCEP/Eta atmospheric model replacing the current Geophysical Fluid Dynamics Laboratory radiation package.

[13] The solar radiation parameterization [*Chou and Suarez*, 1999] includes the absorption due to water vapor, O_3, O_2, CO_2, clouds, and aerosols. Interactions among the absorption and scattering by clouds, aerosols, molecules (Rayleigh scattering), and the surface are fully taken into account. There are eight bands in the ultraviolet and visible region and three bands in the infrared region. Fluxes are integrated virtually over the entire spectrum, from 0.175 μm

Table 1. Spectral Bands in the Solar and Thermal Wavelengths in the Radiation Module

Band Number	Solar Wavelength, μm	Thermal Wave Number, cm^{-1}
1	0.175–0.225	0–340
2	0.225–0.245	340–540
	0.260–0.280	
3	0.245–0.260	540–800
4	0.280–0.295	800–980
5	0.295–0.310	980–1100
6	0.310–0.320	1100–1215
7	0.320–0.400	1215–1380
8	0.400–0.700	1380–1900
9	0.70–1.22	1900–3000
10	1.22–2.27	
11	2.27–10.0	

to 10 μm. Band intervals are listed in Table 1. A maximum-random approximation is adopted for the overlapping of clouds at different heights. Reflection and transmission of a cloud and aerosol-laden layer are computed using the d-Eddington approximation. Fluxes are then computed using the two-stream adding approximation.

[14] The long-wave radiation parameterization [*Chou et al.*, 2001] is based on the 1996 version of the Air Force Geophysical Laboratory HITRAN database [*Rothman et al.*, 1998]. The parameterization includes the absorption due to major gaseous absorption (water vapor, CO_2, O_3) and most of the minor trace gases (N_2O, CH_4, CFCs), as well as clouds and aerosols. The thermal infrared spectrum is divided into nine bands and a subband (from 0 to 3000 cm^{-1}) (Table 1). Scattering due to clouds and aerosols is included by scaling the optical thickness. The gaseous transmission function is computed either using the k-distribution method or a table look-up method.

[15] For a cloud layer the optical thickness is parameterized as a function of cloud water/ice amount and the effective particle radius, whereas the single-scattering albedo and asymmetry factor are parameterized as a function of the effective particle radius. The effective particle radius is, in turn, parameterized as a function of cloud water/ice concentration and temperature. Aerosol optical properties as functions of spectral band, height, and species are input parameters to the radiation routine.

[16] In our new dust-radiation scheme we use eight dust size bins. The bin intervals are taken from *Tegen and Lacis* [1996] as listed in Table 2. Within each transport bin, dust is assumed to have time-invariant, subbin lognormal distribution [*Zender et al.*, 2003] employing the transport mode with mass median diameter of 2.524 μm [*Shettle*, 1984] and a geometric standard deviation of 2.0 [*Schulz et al.*, 1998]. The submicron particles correspond to the clay-originated aerosol (bins 1–4) and the remaining particles to the silt (bins 5–8). At the sources, the clay/silt content is specified according to soil type characteristics evaluated from the Staub and Rosenzweig Zobler Near-Surface Soil Texture data, and the UNEP/GRID Gridded FAO/UNESCO Soil Units [*Nickovic et al.*, 2001]. Grid points acting as desert dust sources are specified using arid and semiarid categories of the global USGS 1-km vegetation data set. Source distribution was derived from *d'Almeida* [1987] [see *Pérez et al.*, 2006].

[17] For each size bin and wavelength we calculate the extinction efficiency, single-scattering albedo and asymmetry factor with a Mie-algorithm based on the work of *Mishchenko et al.* [2002]. Each particle is assumed to be homogeneous and spherical. Although there is sufficient experimental evidence that nonsphericity of desert dust can result in significantly different scattering properties than those predicted by Mie theory [*Mishchenko et al.*, 2000], its effect upon radiative fluxes and albedos is small [*Lacis and Mishchenko*, 1995]. Complex refractive indices are taken from the Global Aerosol Data Set (GADS) [*Koëpke et al.*, 1997] although it has to be signaled that recent in situ measurements of dust absorption at solar wavelengths suggest that the adopted indices of refraction could be excessively absorbing [*Kaufman et al.*, 2001]. Finally, a weighted integration across the spectral band width is done with the extraterrestrial solar irradiance spectrum for the solar wavelengths and the Planck function for long-wave wavelengths.

[18] Mean values of optical thickness (τ), single-scattering albedo (w), and asymmetry factor (g) are in turn derived for each spectral band (Δλ) and atmospheric layer according to

$$\tau(\Delta\lambda) = \sum_{k=1}^{8} \tau_k(\Delta\lambda) = \sum_{1}^{8} \frac{3}{4\rho_k r_k} M_k Q_{ext}(\Delta\lambda)_k \tag{1}$$

$$w(\Delta\lambda) = \frac{\sum_{k=1}^{8} w_k(\Delta\lambda)\tau_k(\Delta\lambda)}{\sum_{k=1}^{8} \tau_k(\Delta\lambda)} \tag{2}$$

$$g(\Delta\lambda) = \frac{\sum_{k=1}^{8} g_k(\Delta\lambda) w_k(\Delta\lambda)\tau_k(\Delta\lambda)}{\sum_{k=1}^{8} \tau_k(\Delta\lambda) w_k(\Delta\lambda)} \tag{3}$$

where for each size bin k: ρ is the particle mass density, r is the effective radius, M is the layer mass loading, and Q_{ext} is the extinction efficiency. Figure 1 displays the calculated extinction efficiency, single-scattering albedo, and asymmetry factor for four size bins at the 11 solar bands and the 9 thermal bands outlining their strong dependence on particle size.

2.3. Experimental Design

[19] We selected a major dust outbreak that occurred over the Mediterranean region during the period 8–15 April

Table 2. Dust Size Bins Introduced in the Model[a]

Bin Number	r_{min}-r_{max}, μm	r_{eff}, μm
1	0.1–0.18	0.15
2	0.18–0.3	0.25
3	0.3–0.6	0.45
4	0.6–1	0.78
5	1–1.8	1.3
6	1.8–3	2.2
7	3–6	3.8
8	6–10	7.1

[a]Here r_{min}-r_{max} are minimum and maximum radius and r_{eff} is effective radius for each size bin.

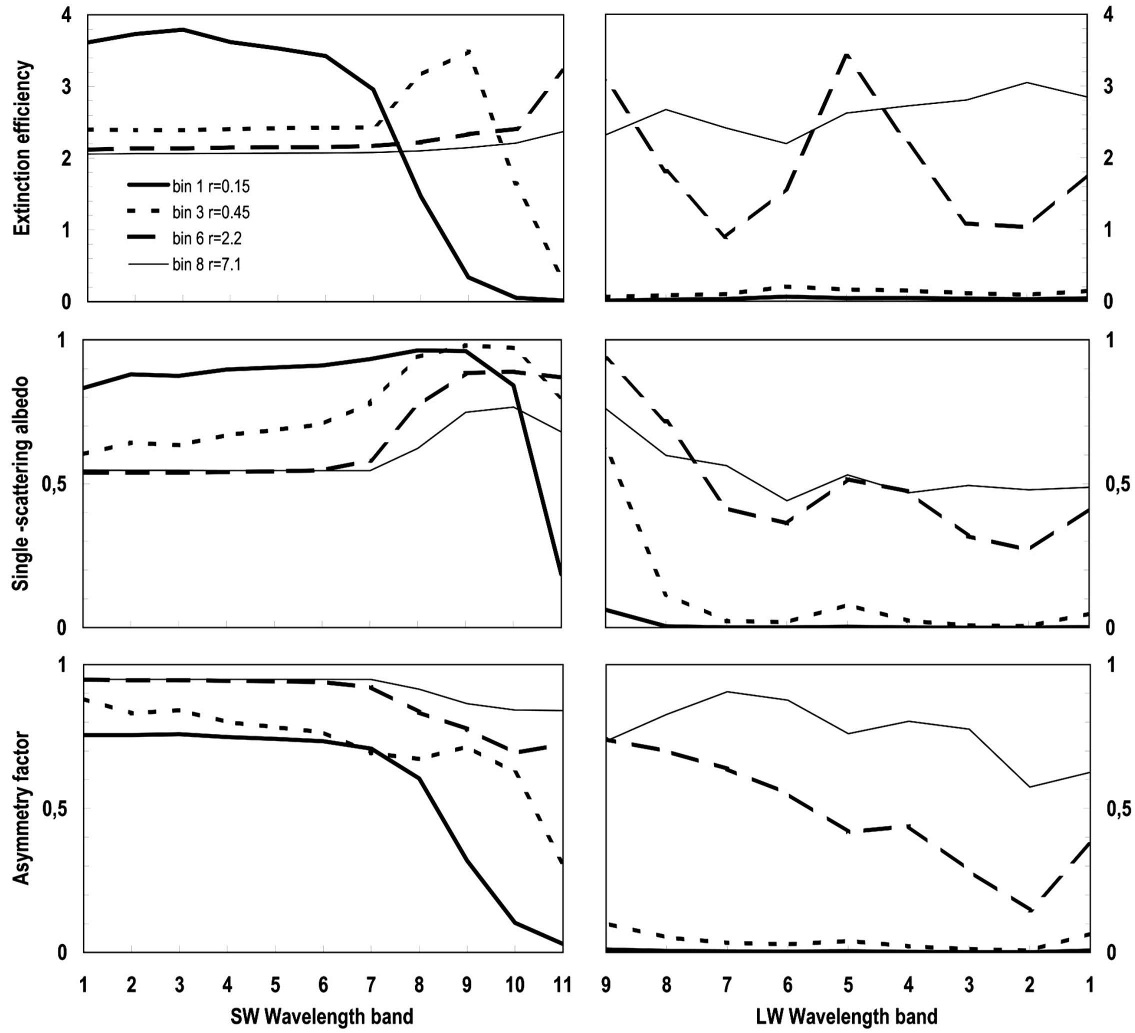

Figure 1. Input radiative parameters for the solar and long-wave radiation packages for dust size bins 1, 3, 6, and 8 as a function of spectral band. The band and bin intervals are specified in Table 1 and 2, respectively.

2002 and we performed two sensitivity experiments. In the control experiment (hereafter referred to as CTR), dust has been considered as a dynamic tracer without interaction with atmospheric radiation. In the other experiment (hereafter referred to as RAD), interaction between short- and long-wave radiation and dust is included.

[20] Since there are not yet satisfactory three-dimensional dust concentration observations to be assimilated, the initial state of dust concentration in the model is defined by the 24-hour forecast from the previous-day model run. Only in the "cold start" of the model, concentration is set to zero. The cold start of the model was initiated on the 5 April 2002. The resolution is set to 50 km in the horizontal and to 24 layers extending up to approximately 15 km in the vertical. The domain of simulation covers northern Africa, the Mediterranean Sea, and southern Europe (Figure 2).

3. Results and Discussion

3.1. April 2002 Dust Outbreak in the Mediterranean

[21] Over this period, the major dust influxes were generated over Morocco, Western Sahara, northern Mauritania, northern and southern Algeria, Tunisia, and northern Libya. Once lifted into the atmosphere, dust was transported to the northeast, emerging of the north African coast on 9 April. Figure 2 shows the objective analysis of the mean sea level pressure and the wind vectors at 3000 m on 12 April indicating a deep cyclonic activity over the western Mediterranean. SE wind speed in the central Mediterranean exceeded 20 m/s at midlevels providing fast transport of dust away from the sources. Figure 3a shows the predicted aerosol optical depth (AOD) and cloud cover on the 11, 12, and 13 April depicting the evolution of both dust and cloud processes over the area. Also shown are the corresponding SeaWIFS satellite images, which confirm reasonable accuracy of the simulation. Strong AOD values between 2.5 and 3.5 at 550 nm were reached over northern Algeria and over the western Mediterranean Sea on 11 April and over Tunisia and the central Mediterranean on 12 and 13 April. Sensor MODIS AOD retrievals confirmed the range of values obtained (not shown). During the period, cloudiness was mainly confined to the European continent and the Mediterranean Sea.

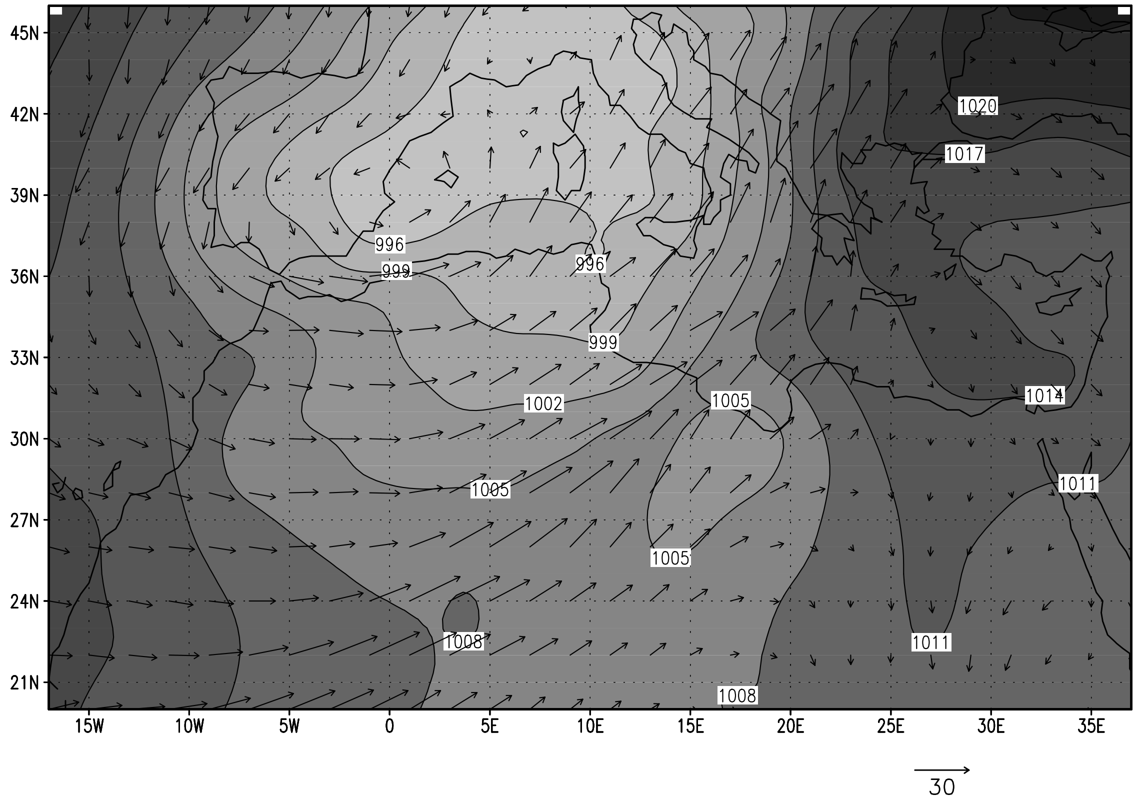

Figure 2. Analysis of the mean sea level pressure and wind vectors at 3000 m on 12 April at 1200 UTC.

[22] The vertical dust concentration distribution is crucial for accurate calculations of radiative heating/cooling rates [*Sokolik and Golitsyn*, 1993]. DREAM has demonstrated its capability to assess with reasonable accuracy the dust vertical structure over the Mediterranean region in the intensive comparisons with lidar data [*Pérez et al.*, 2006]. In this study we limit ourselves to compare the predicted vertical profiles of the extinction coefficient at 350 nm with one aerosol lidar station at Napoli (Italy) affected by the considered dust event (Figure 4). Napoli is one of the 20 stations within the European Aerosol Research Lidar Network (EARLINET) [*Bösenberg et al.*, 2003] intercalibrated in several campaigns to ensure high-quality data [*Böckmann et al.*, 2004; *Matthias et al.*, 2004]. The lidar profiles of the extinction coefficient reached values up to 1000 Mm^{-1} showing highly complex vertical structure of the dust on the 12 April. In comparison with lidar data, the model fairly well captured the main dust pattern and showed an exceptional behavior on the 11 and 13 April.

3.2. Dust Impact on Atmospheric Processes

3.2.1. Radiative Forcing

[23] The radiative forcing was calculated as instantaneous flux differences between the two simulations (RAD and CTR). The geographic distribution of the instantaneous net, short-wave and long-wave forcing at the surface and the top-of-atmosphere (TOA) on 12 April at 1200 UTC is shown in Figure 5. The averages over the whole domain of simulation at 0000, 0600, 1200, and 1800 UTC in the period 11–13 April are depicted in Figure 6.

[24] The net surface forcing is the result of scattering of the shortwave sunlight by absorption and backscattering during the daytime and of the all-day long-wave gain of radiation by emission of dust. As shown in Figure 5, the geographic distribution of the net surface forcing during the day mainly follows the variations in the dust AOD being more negative where the dust loading is more intense. Minimum instantaneous negative values reached less than -600 W/m^2 over Tunisia where the AOD was 3.5 at 550 nm. Minimum domain-average net negative forcing remained above -50 Wm^{-2} at 0600 UTC and within -100 and -130 Wm^{-2} at 1200 UTC. As outlined by global dust modeling sensitivity experiments in the work of *Miller et al.* [2004b], the consideration of less dust short-wave absorption [*Kaufman et al.*, 2001] would result in less negative surface forcing. Positive forcing spots over the western side of the domain correspond to changes in the cloud distribution. The long-wave domain-average surface positive forcing is only slightly balanced by the shortwave negative forcing resulting to a small net positive forcing over the night (Figure 6).

[25] The geographic distribution of the TOA forcing mainly follows the variations in the dust AOD and the properties of the underlying surface. Minimum instantaneous negative values of about -200 Wm^{-2} were reached at 1200 UTC over the central Mediterranean Sea in cloud-free areas highly loaded by dust (AOD values of 3). The negative forcing is a result of increased columnar reflectance over the relatively dark sea which would be larger if considering less dust short-wave absorption. Maximum instantaneous positive values were reached in dust-affected areas over land due to increased columnar absorption over the bright land surface. Even higher values were achieved

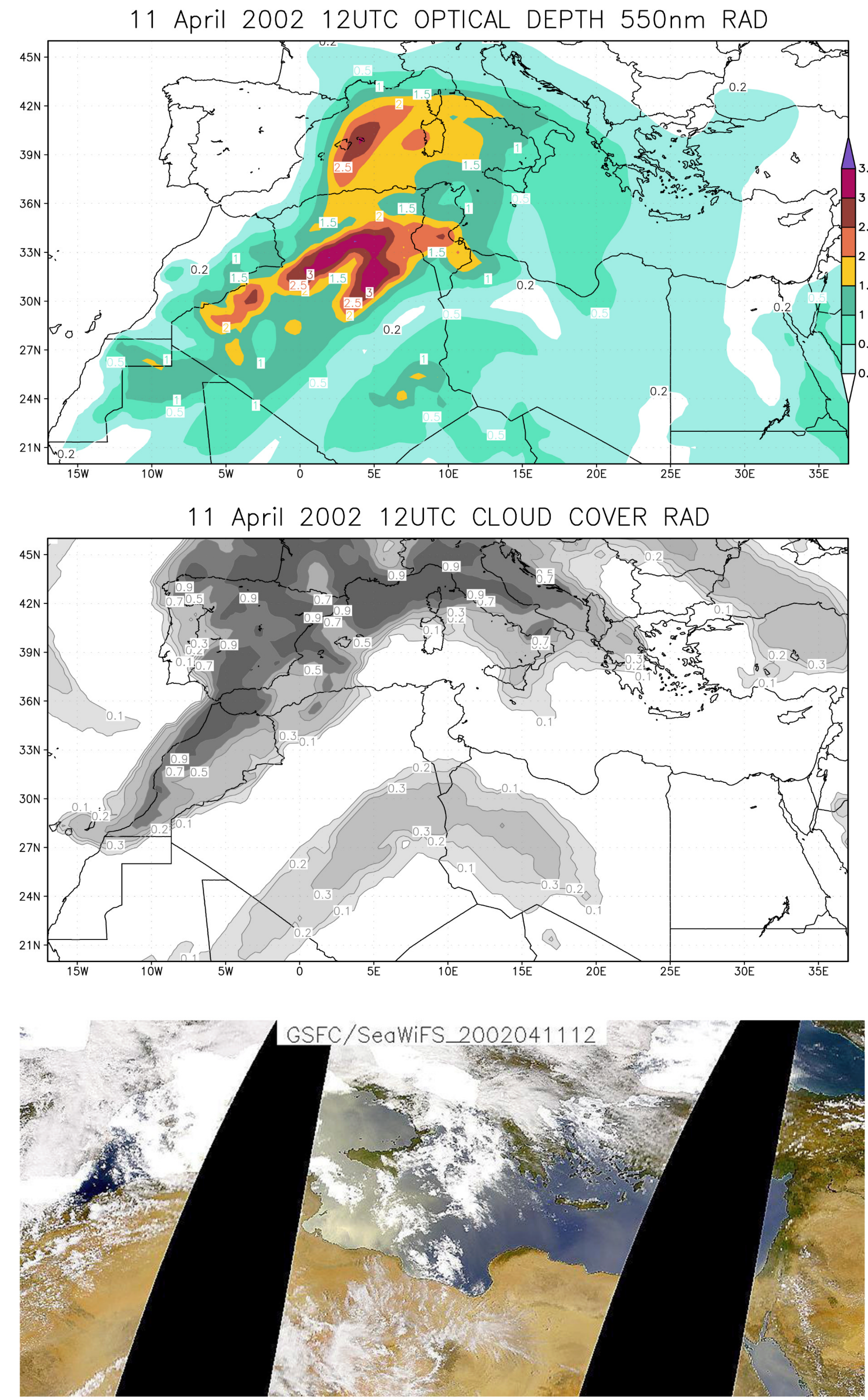

Figure 3a. From up to down: modeled AOD at 550 nm, modeled cloud cover with RAD experiment and SeaWIFS satellite image on 11 April at 1200 UTC.

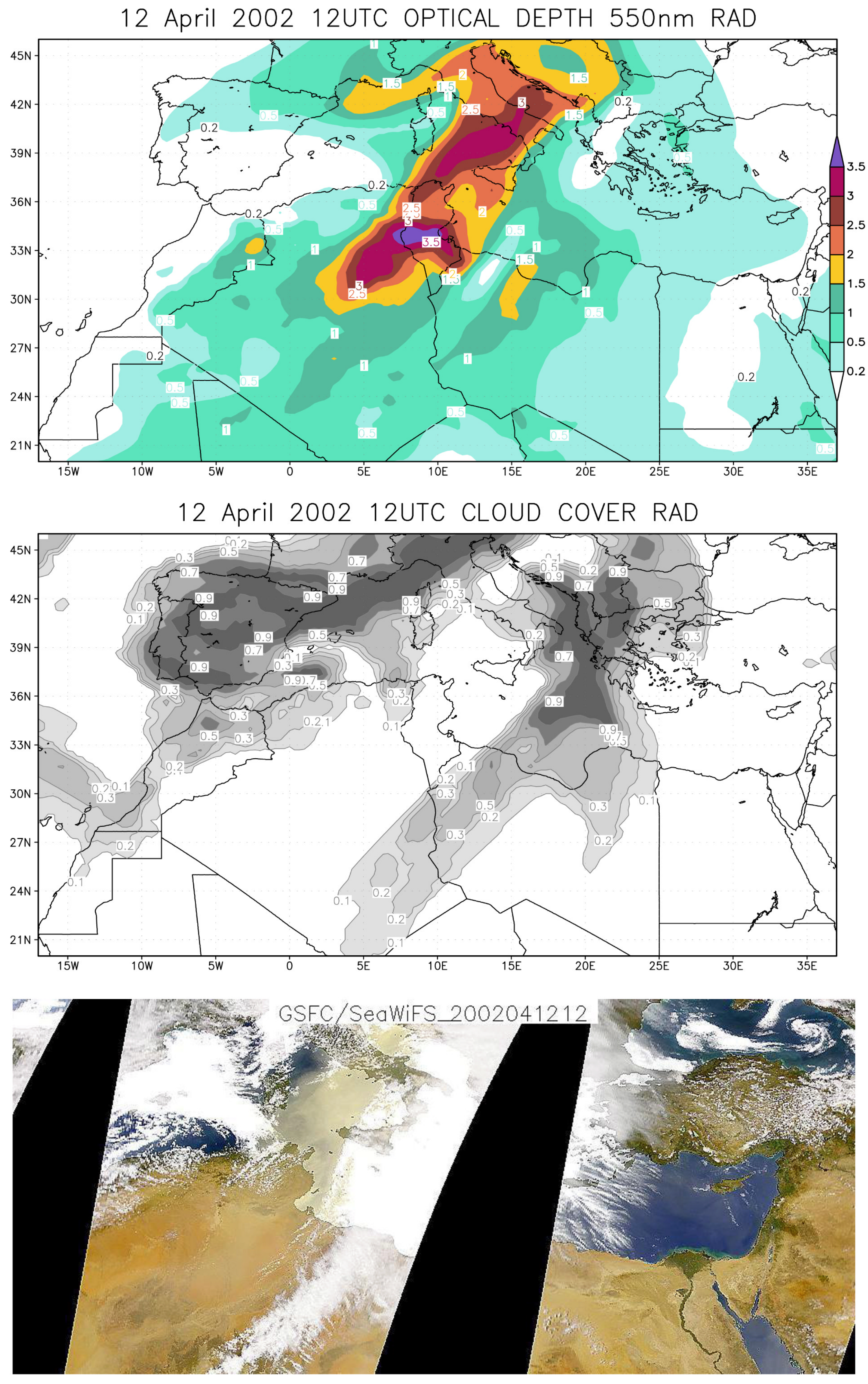

Figure 3b. Same as Figure 3a on 12 April at 1200 UTC.

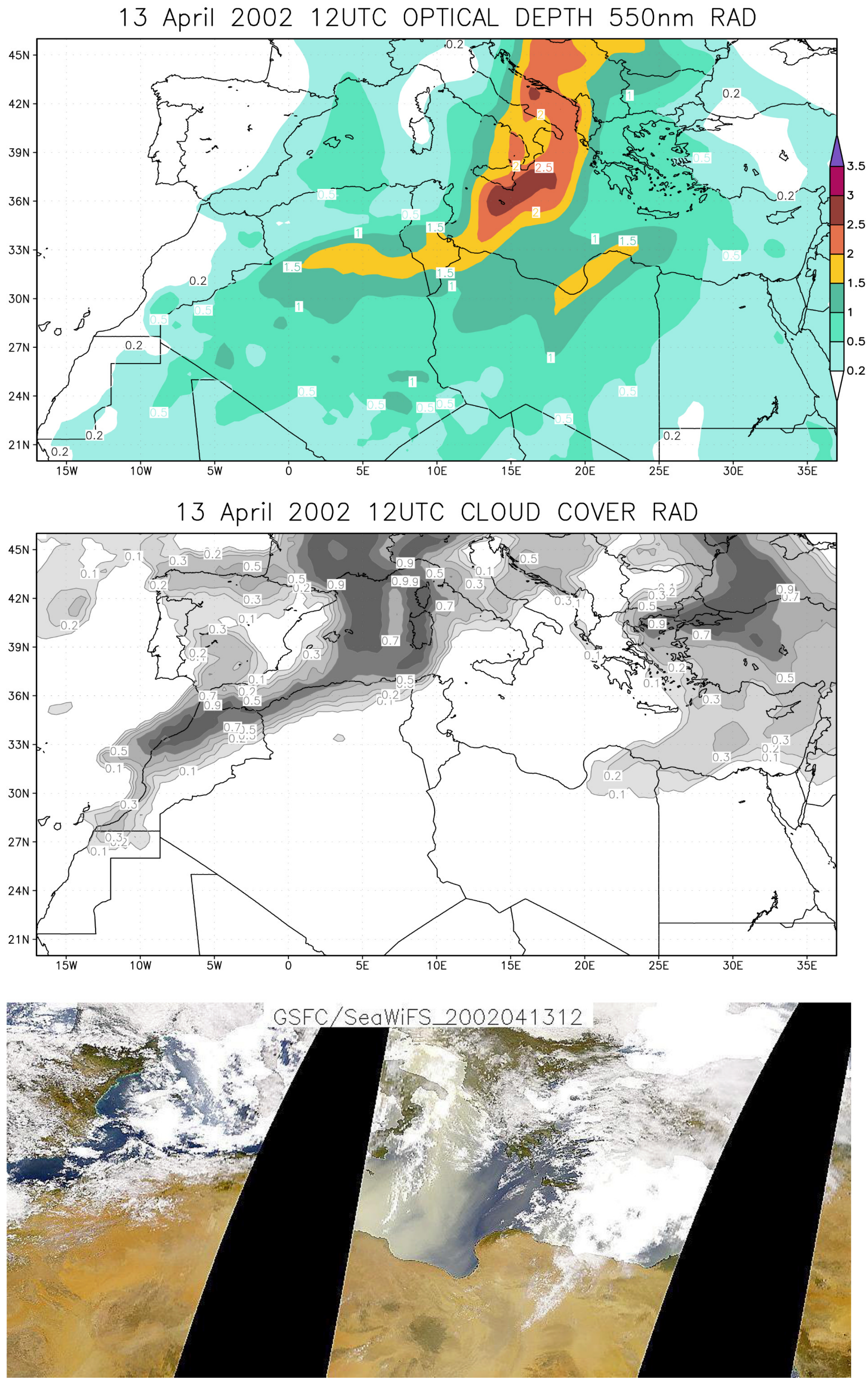

Figure 3c. Same as Figure 3a on 13 April at 1200 UTC.

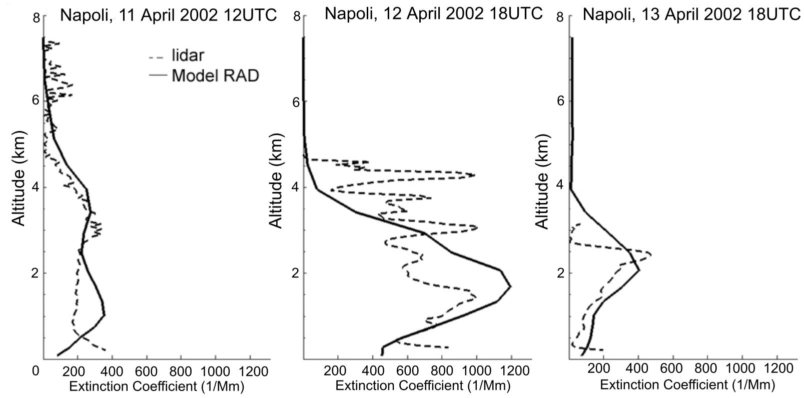

Figure 4. Modeled and lidar profiles of the extinction coefficient at 350 nm over Napoli (Italy) on 11 (left), 12 (center), and 13 (right) April 2002.

over land areas affected by both dust and clouds. On the other hand, there is a positive forcing over the sea in areas where dust and clouds coexisted (the Adriatic Sea and the northwestern Mediterranean Sea). The domain-average net TOA forcing was always positive with maximum values of about 50 Wm^{-2} at 1200 UTC. The TOA forcing is small in comparison to the surface forcing because the absorption of dust aerosols reduces the net flux beneath the dust layer to a greater extent than the net flux above.

[26] The net atmospheric forcing, defined as the difference between the TOA and surface forcing, shows how dust radiatively heated the column over land and sea with maximum instantaneous values over the former of about 700 Wm^{-2}. The overall effect over the domain was positive during the day reaching almost 160 Wm^{-2} and being slightly negative during the night.

3.2.2. Turbulent Fluxes and Dust Negative Feedback

[27] In GCM experiments of *Perlwitz et al.* [2001] the effect of dust radiative forcing was to reduce the global dust load by roughly 15% for the present climate. *Miller et al.* [2004a] explored the mechanisms of interaction between dust radiative forcing and boundary layer processes. They found that by reducing sunlight upon the surface, dust decreases the turbulent mixing within the PBL and consequently the downward transport of momentum to the surface, resulting in a decrease of surface wind speed and dust emission. As they pointed out, this negative feedback was underestimated by the low-resolution GCM (4° latitude by 5° longitude) partly because the model neglected wind speed fluctuations on smaller and more rapid timescales. In our case study we explore these mechanisms using much higher model resolution and including more sophisticated turbulent and surface emission schemes.

[28] In our experiments, there is a high dust spatial correlation of about 0.95 between CTR and RAD on 12 April (not shown). However, the inclusion of dust-radiation interactions reduced by 35–45 % the average AOD over the area covered by the main dust plume, indicating a strong negative feedback upon dust emission by dust radiative forcing (Figure 7).

[29] Figures 8a and 8b show scatter plots of differences of the sensible and latent heat fluxes with respect to the instantaneous net surface forcing by dust over northern Africa on 12 April. As previously outlined, the surface forcing was strongly negative during the day and slightly positive during the night. The reduction of the sensible heat flux is strongly correlated to the net surface forcing (determination coefficient is 0.95) and very large (regression coefficient is 0.79) during the day when turbulence is fully developed (Figure 8a). At night the determination and regression coefficients drop to 0.72 and 0.47, respectively (Figure 8b). The reduction of the latent heat flux is nonlinear and rather small due to its dependency on soil moisture availability and to the general dry soil conditions over desert areas. Thus the negative net surface forcing during the day is mainly balanced by the reduction of the turbulent sensible heat flux to the atmosphere, which in turn reduces the amount of turbulent kinetic energy (TKE) into the PBL. The vertical turbulence exchange in the NCEP/Eta model uses the Mellor-Yamada-Janjic Level 2.5 scheme [*Janjic*, 2001]. In this approach, the TKE is a fully prognostic variable and is used to compute the turbulent exchange coefficients for the transfer of heat, moisture, and momentum between adjacent model layers.

[30] In dust models, either surface flux or surface concentration can be used as a lower boundary condition. In DREAM the concentration as a surface condition is used in order to be consistent the NCEP/Eta approach for moisture and heat flux (schemes that use surface parameters as a lower boundary condition). The released surface concentration depends on a dust productivity factor, which takes into account effects of soil structure and particle size distribution. The surface concentration is a second power function of the friction velocity (third power for the flux) thus depending strongly on surface turbulent conditions. Furthermore, the threshold friction velocity bellow which dust injection is ceased depends on soil wetness and particle size [*Nickovic et al.*, 2001]. Figure 8c outlines a rather strong relationship between the reduction in friction velocity and surface forcing during the day (determination coefficient is 0.54).

[31] Surface turbulent momentum exchange coefficients are calculated following the Monin-Obukhov theory [*Janjic*, 1996a]. Figures 8d and 8e show a strong correlation between reduction in the turbulent exchange coefficients for momentum and heat (0.69, 0.76) and surface forcing. These coefficients are used in the emission parameterization scheme of the model. In this scheme, viscous sublayer

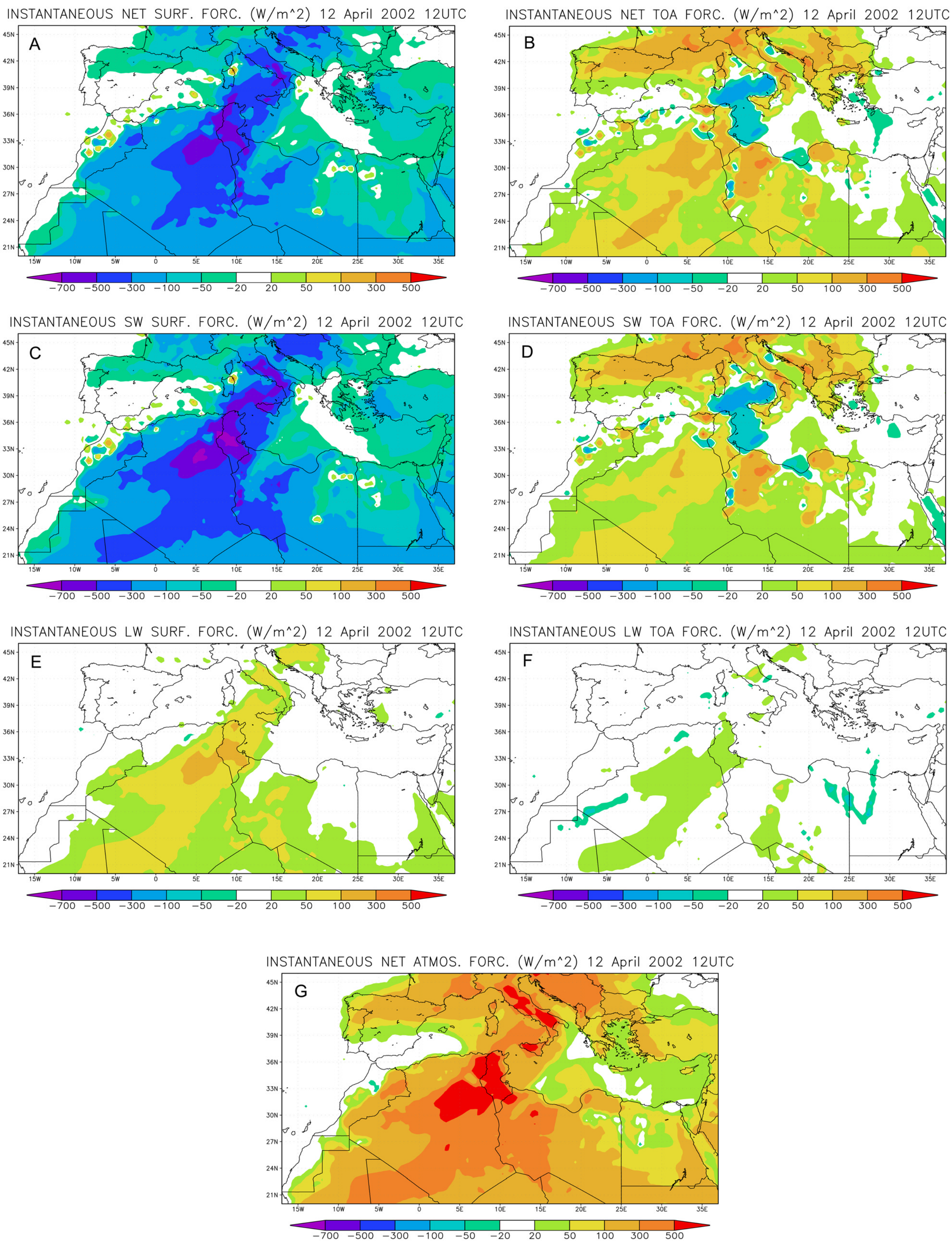

Figure 5. Instantaneous forcing by dust aerosols on 12 April 2002 at 1200 UTC (Wm^{-2}): (a) net surface, (b) net TOA, (c) shortwave surface, (d) shortwave TOA, (e) longwave surface, (f) longwave TOA, (g) net atmospheric.

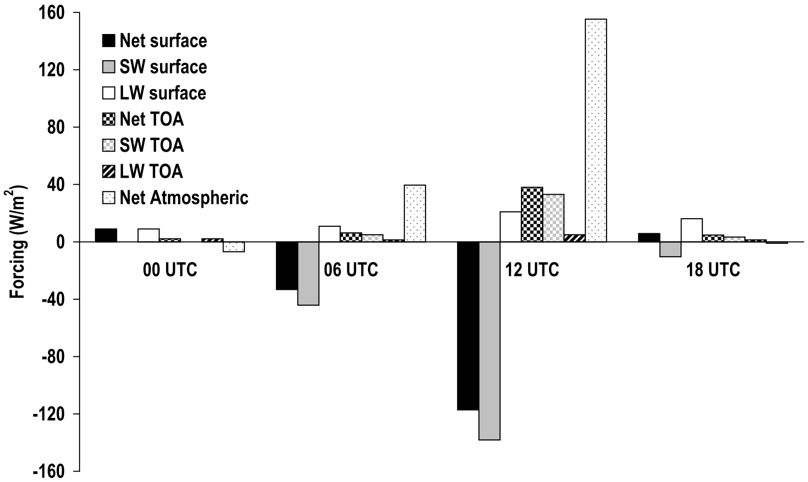

Figure 6. Instantaneous net, shortwave (SW) and longwave (LW) forcing at the surface and the TOA and net atmospheric forcing averaged over the whole domain of simulation at 0000, 0600, 1200, and 1800 UTC on the period 11–13 April 2002.

effects are taken into account in the dust production following the viscous sublayer scheme of *Janjic* [1994]. On the basis of a physical similarity of mass/heat/momentum exchange over surfaces with mobilized particles such as sea, snow, and desert surfaces [*Chamberlain*, 1983; *Segal*, 1990], *Nickovic et al.* [2001] applied the Janjic scheme in the dust production part of the model. The viscous sublayer appears as a physical mechanism that regulates if mass/heat/momentum exchange at the air-ground surfaces with mobilized elements is dominated by turbulent or laminar mixing. In DREAM the surface fluxes for each size bin k in the viscous sublayer scheme are calculated as

$$F_{S_k} = K_S^* \frac{C_{LM_k} - C_{S_k}}{\Delta z} \tag{4}$$

where C_{LMk} is the concentration at the lowest model level, C_{sk} is the surface concentration, Δz is the depth of the lowest model level, and

$$K_S^* = \frac{1}{1+w} K_S \tag{5}$$

is a conventional similarity-theory turbulent exchange coefficient corrected by viscous effects. K_s is the turbulent exchange coefficient for concentration which is defined to be identical to turbulent exchange coefficients for heat and moisture. In (5), w is a function of the viscous sublayer depth (see *Nickovic et al.* [2001] for details) which has a role of weighting factor depending on the type of turbulent regime. The viscous sublayer for dust operates in three regimes: smooth, rough, and very rough. Regime transitions are assumed to occur at 0.225 and 0.7 ms^{-1}. Under very rough conditions, the viscous sublayer for dust is completely ceased and fully developed turbulence is the only mixing mechanism, leading to extensive injection of dust.

[32] The response of dust flux to surface forcing is not straightforward being highly nonlinear function of surface turbulent conditions as shown in Figure 8f. However, there is an overall reduction in dust flux during the day that can be very large over emission areas reaching up to -0.4 mg m^{-2} s^{-1} versus -300 Wm^{-2}.

3.2.3. Improved Accuracy of the Forecasted Weather

[33] It is expected that inclusion of the radiative effects of mineral dust could improve the radiation balance of NWP models and consequently contribute to a better accuracy of the weather prediction itself. *Geleyn and Tanré* [1994] pointed out in their short-term modeling study that mineral dust has a recognizable impact on large-scale dynamics. Recently, *Kischa et al.* [2003] related systematic short-term temperature forecast errors to the absence of dust radiative effects in models over the Saharan region. *Haywood et al.* [2005] stated that the neglection of mineral dust in a NWP model is the most probable reason for the discrepancy in outgoing longwave radiation between the model and Meteosat-7 observations over northern Africa. Dust could have contributed to a long-wave radiative monthly mean forcing of as much as 50 Wm^{-2}.

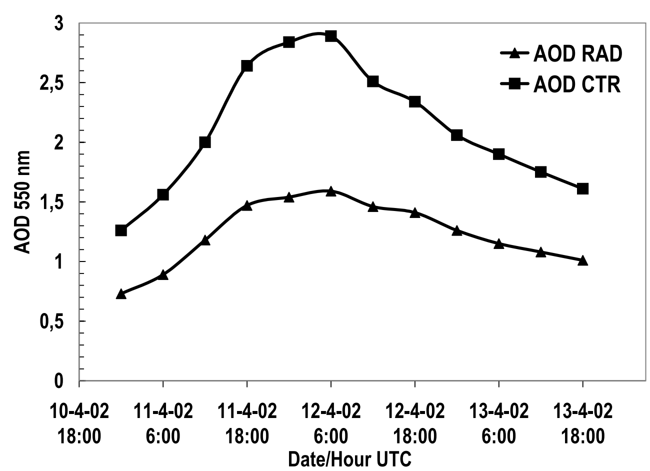

Figure 7. Average AOD at 550 nm over the area between latitude 30°N–45°N and longitude 0–20°E on the period 11–13 April 2002 with RAD and CTR experiments.

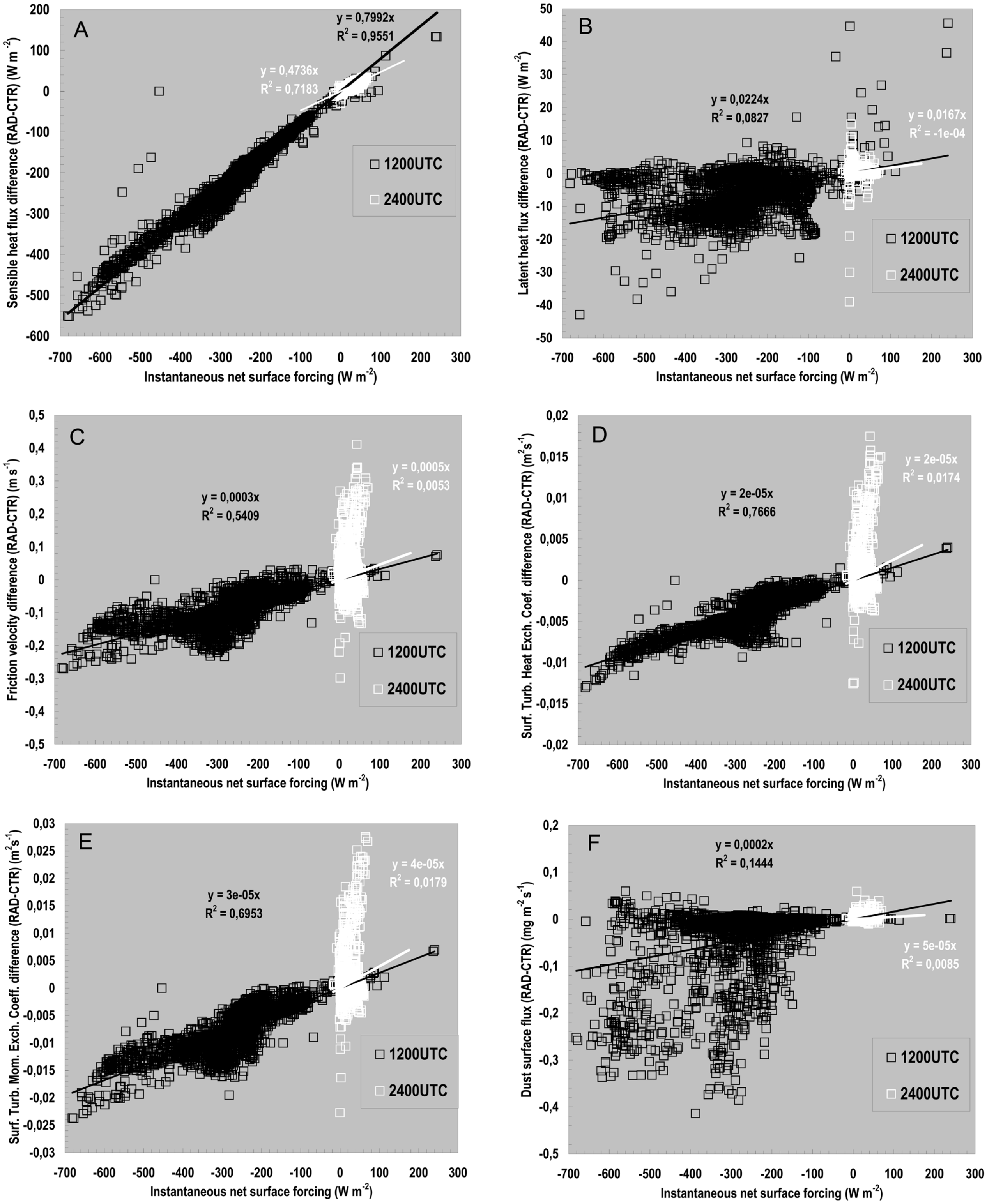

Figure 8. Scatterplots and regression lines of the instantaneous net surface forcing with respect to instantaneous differences between RAD and CTR of (a) surface sensible heat flux to the atmosphere, (b) latent heat flux to the atmosphere, (c) friction velocity, (d) surface turbulent heat exchange coefficient, (e) surface turbulent momentum exchange coefficient, (f) dust flux to the atmosphere, on 12 April at 1200 UTC and on 13 April at 0000 UTC, over northern Africa between latitude 20°N–35°N and longitude 6°W–10°E.

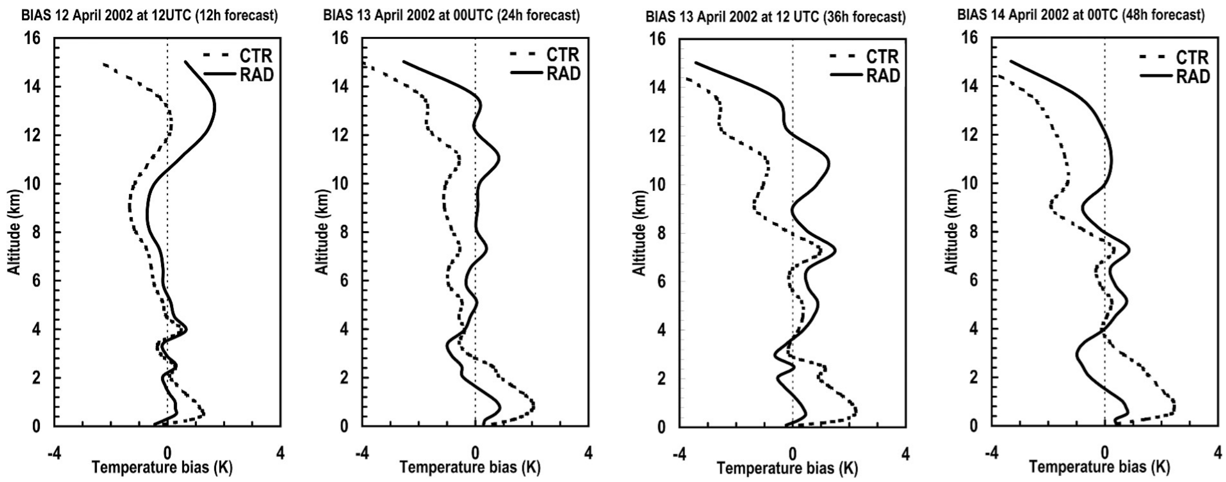

Figure 9. Atmospheric temperature bias of CTR and RAD over the main dust-affected area (comprised between latitude 30°N to 45°N and longitude 0 to 20°E) for the 12, 24, 38, and 48 hour forecasts of the 0000 UTC cycle on 12 April.

[34] In our study the temperature forecasts by RAD and CTR are validated against objective analysis data. Figure 9 depicts the atmospheric temperature bias (defined as modeled minus observed value) computed over the main dust-affected area (comprised between latitude 30°N to 45°N and longitude 0 to 20°E) using the 12, 24, 36, and 48 hour forecasts of the 0000 UTC cycle on 12 April.

[35] The CTR temperature forecasts show a strong warm bias in the lower troposphere (up to 2.5 K) and a strong cold bias in the upper atmosphere (up to 4 K). The RAD temperature profiles improve the CTR bias scores in most of the atmospheric layers. This is clearly visible for the 24 hour forecast where the bias approaches 0 K between 4 and 14-km height. Here, it achieves slightly worse scores between 2.5 and 4 km and at 11 km while it considerably improves scores below 2 km and above 14 km. For the 36 hour and 48 hour forecasts RAD has higher midlevel bias but they are small when compared to the improvements achieved in upper and lower levels. The most striking feature is that the overall effect of dust is the reduction of both CTR warm and cold biases by heating the upper atmosphere and cooling the lower troposphere, respectively.

[36] The simulated cooling of the lower atmosphere where the major dust pattern is located cannot be explained by pure static 1-D radiative transfer considerations. Many studies show that increasing dust loading results in a net heating of the dust layer [e.g., *Quijano et al.*, 2000]. In order to explain the main reasons for the model performance that we obtained, Figure 10 displays a north to south vertical cross-section of the extinction coefficient at 550 nm and the atmospheric temperature difference between RAD and CTR over a cloud-free area on 12 April at 1200 UTC. Also shown is the horizontal distribution of 2-m temperature difference over the whole domain. First, it should be noted that over land the negative radiative forcing at the surface significantly reduces the sensible heat flux to the atmosphere, which in turn reduces the PBL temperature (differences in 2 m temperature can reach 6 K in some areas). These effects completely offset the dust radiative heating through solar absorption near the surface. Dust redistributes heat from the surface and near surface to higher levels of the atmosphere.

[37] Concerning the atmospheric temperature over the sea within the whole dust layer, two competing effects are found. Namely, close to the African coast (between 34°N and 37°N), the air cooled by the dust over land (as described above) is advected by the prevailing southern winds (not shown) leading to negative temperature difference in the vicinity of the Tunisian and Libyan coast. However, the radiative heating by dust absorption prevails further to the north (between 39°N and 40°N).

[38] As introduced in section 2.2, the RAD experiment was performed assuming dust optical properties from the Global Aerosol Data Set. However, some studies suggest that dust is less absorbing [*Kaufman et al.*, 2001]. *Miller et al.* [2004b] performed sensitivity experiments showing that a 10% decrease in the single scattering albedo (corresponding to an increase of absorption) results in a 50% increase in the magnitude of the surface forcing. Also, the radiative heating doubles for a 10% reduction in the single scattering albedo, even in the upper troposphere. The assumption of less absorbing dust would then result in a reduction of the atmospheric radiative heating and the negative surface forcing. In our context the cold bias in the upper troposphere would not be reduced as much as in the current RAD experiment. In the lower troposphere, the effect on the warm bias would be the result of the balance among an increased outgoing sensible heat flux and a decreased radiative heating with respect to more absorbing dust.

[39] The RAD radiative balance is further affected through the semidirect effect of dust. Although explicit cloud-dust microphysical interactions are not included in this study, clouds are still affected "semidirectly" by the thermal and dynamic impacts of dust. The experiments show that cloud patterns, which are mainly confined to the northern part of the domain, increasingly differ in horizontal structure and amount. Figure 11 displays the average cloud fraction difference between RAD and CTR

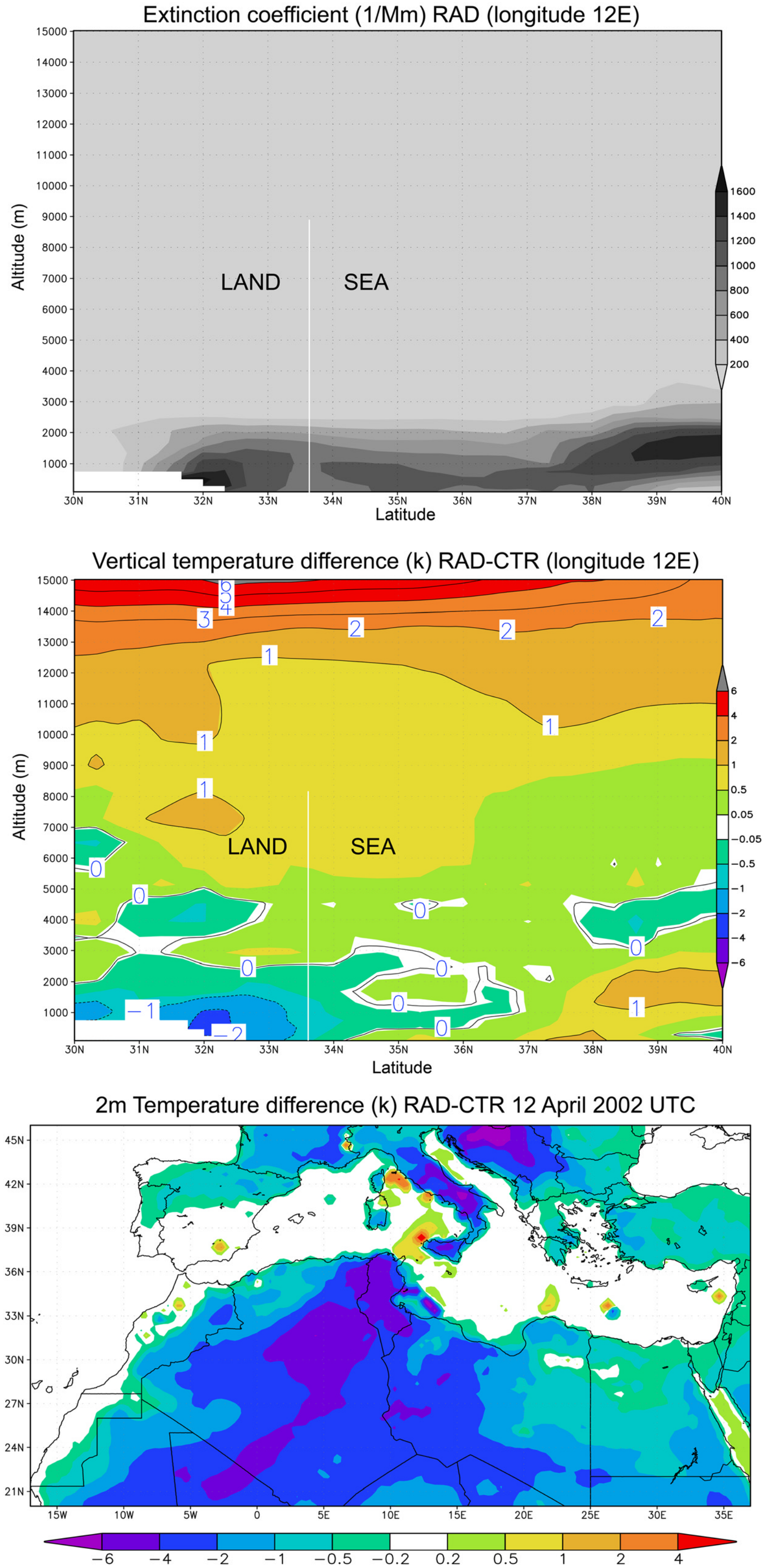

Figure 10. Vertical cross-sections between latitudes 30°N and 40°N along longitude 12°E of (a) the extinction coefficient at 550 nm from RAD and (b) the atmospheric temperature difference between RAD and CTR on the 12 April 2002 at 1200 UTC. (c) Horizontal distribution of 2m temperature difference over the whole domain.

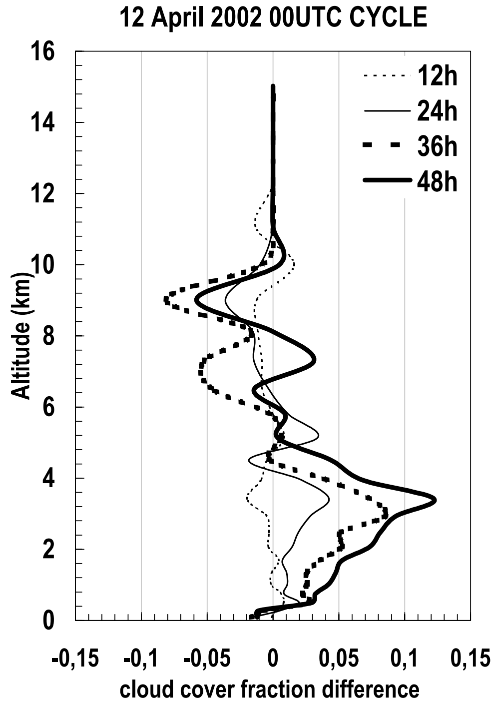

Figure 11. Cloud cover fraction difference between CTR and RAD over the main dust-affected area (comprised between latitude 30°N to 45°N and longitude 0 to 20°E) for the 12, 24, 38, and 48 hour forecasts of the 0000 UTC cycle on 12 April.

of the 12, 24, 36, and 48 hour forecasts outlining for this case the tendency of dust to enhance low and midlevel clouds and reducing high-level clouds. This further changes precipitation and wet deposition patterns. These effects will be further explored in a forthcoming contribution.

[40] The thermal forcing of the atmosphere perturbs the atmospheric circulation. *Overpeck et al.* [1996] showed that the presence of tropospheric dust was associated with changes in atmospheric pressure and circulation patterns. Changes in the atmospheric dynamics lead to mean sea level pressure differences between RAD and CTR as shown in Figure 10 for 12 April at 1200 UTC (Figure 12). We obtain positive differences over land and negative differences over the sea. The colder atmosphere over land suppresses convection and increases subsidence. The opposite effects are obtained over the sea. The root mean square errors of the sea level pressure forecasts when compared to the objective analysis were calculated over the whole domain for the 0000 UTC cycle on 12 April. The results are indicated in Table 3 showing significant improvement from 24 to 48 hour forecasts.

4. Conclusions

[41] In this study we have incorporated the radiative effects of mineral dust into the NCEP/Eta NWP limited-area model. The new dust-radiation scheme was tested for a major dust outbreak over the Mediterranean on April 2002 in order to assess dust impacts on regional numerical weather forecasting. The dust model experiments demonstrate high agreement with lidar and satellite observations over the central Mediterranean. It has been shown that the newly developed dust-radiation interaction scheme increases accuracy of both atmospheric temperature and

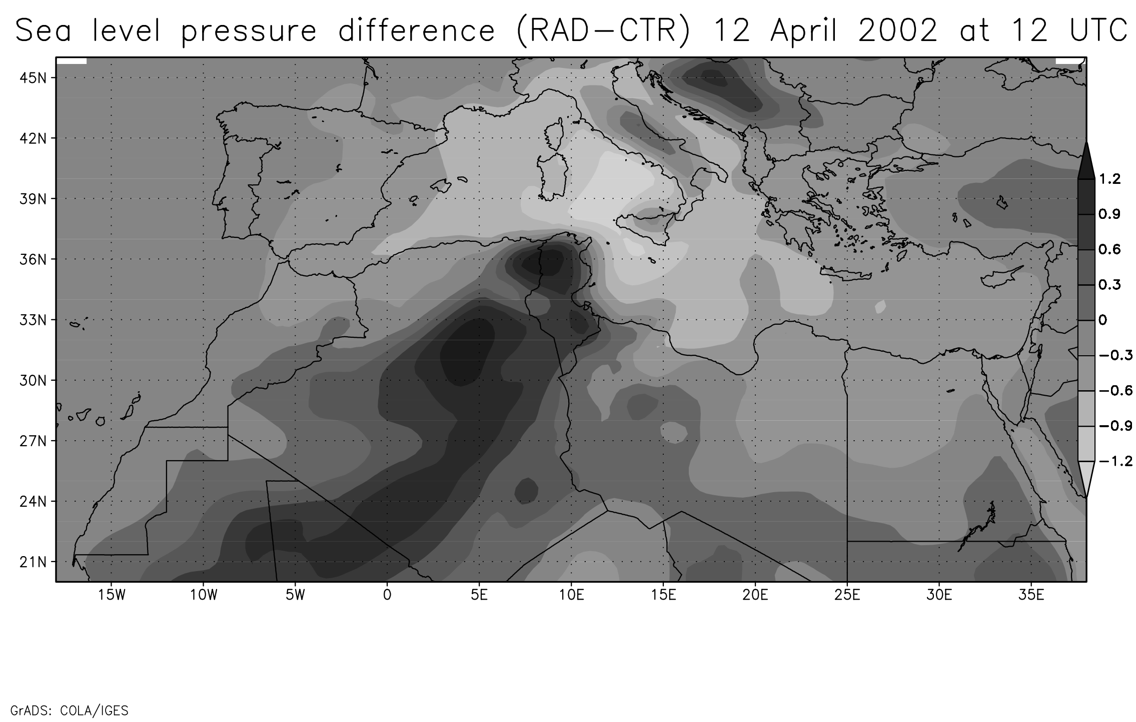

Figure 12. Sea level pressure difference between RAD and CTR on 12 April at 1200 UTC.

Table 3. Root Mean Square Error of the Mean Sea Level Pressure Forecasts at 12, 24, 36 and 48 Hours of the 0000 UTC Cycle on 12 April

	Forecast Time			
Experiment	12 Hours	24 Hours	36 Hours	48 Hours
RAD	1.93	1.52	2.29	1.76
CTR	1.95	1.83	2.73	2.09

mean sea-level pressure forecasts. Both low-level warm and upper-level cold temperature biases are reduced when dust affects the atmosphere thermodynamics. The root mean square error of the mean sea level pressure over the whole domain was reduced by almost 20%.

[42] Moreover, the results outline a strong dust negative feedback upon dust emission. Indeed, the resulting smaller outgoing sensible turbulent heat flux reduces both the turbulent momentum transfer from the atmosphere and dust emission. As a result of the negative feedback on dust emission, the area average of AOD over dust-covered regions is highly reduced. Our emission scheme depends on turbulent viscous sublayer effects and takes into account smaller and more rapid timescales, which are not resolved in GCMs.

[43] We assume that the use of interactive dust-radiation parameterization schemes of the type we propose could be a step forward in improving the accuracy of numerical weather prediction and radiative impact assessments over dust-affected areas.

[44] However, the study has several limitations that should be improved in the future. Currently, the size bin distribution includes dust particles smaller than 10 μm. Although the lifetime of larger particles is short, they still could significantly modify the radiative balance over emission areas. Thus it is planned to extend the range of particle toward larger particles. Furthermore, the use of the assumption of spherical particles will be examined in future tests. Currently, the optical properties of dust, although a function of location, are calculated with refractive indexes from the Global Aerosol Data Set. Future refinements could be obtained using data from intensive observational campaigns such as the ongoing Saharan Mineral Dust Experiment (SAMUM).

[45] The pathways by which aerosols can affect clouds represent one of the largest uncertainties in understanding the climate forcing [*Kaufman et al.*, 2005]. In our experiments, clouds were affected only "semidirectly" through the thermal and dynamic impact of dust. The experiments showed differences in cloud horizontal structure and amount. These effects will be explored with extended seasonal model simulations and by introducing explicit cloud-dust microphysical interactions.

[46] **Acknowledgments.** This work was developed under the research contract REN2003-09753-C02 of the Spanish Ministry of Education and Science. This work was also partly funded by National Aeronautics and Space Administration (NASA) under the Project "Public Health Applications in Remote Sensing (PHAiRS)" and by the European Union Project "Climatology of aerosol dispersion in the Aral Sea region (ARAL-KUM)." The authors gratefully acknowledge the Napoli EARLINET station for providing the lidar profiles, the SeaWIFS-NASA project for providing satellite images and Michael Mischenko for providing the Mie code used to compute the dust optical properties.

References

Böckmann, C., et al. (2004), Aerosol Lidar intercomparison in the framework of the EARLINET project: 2. Aerosol backscatter algorithms, *Appl. Opt.*, *43*, 977–989.

Bösenberg, J., et al. (2003), EARLINET: A European Aerosol Research Lidar Network, *Rep. 348, MPI Rep. 337*, 191 pp., Max-Planck-Inst. für Meteorol., Hamburg.

Chamberlain, A. C. (1983), Roughness length of sea, sand, and snow, *Boundary Layer Meteorol.*, *25*, 405–409.

Chou, M. D., and M. J. Suarez (1999), A solar radiation parameterization for atmospheric studies, *NASA Tech. Memo. 15 (10,460)*, 42 pp., NASA, Washington, D.C.

Chou, M. D., M. J. Suarez, X. Z. Liang, and M. M. H. Yan (2001), A thermal infrared radiation parameterization for atmospheric studies, *NASA Tech. Memo. 19 (10,4606)*, 55 pp., NASA, Washington, D.C.

d'Almeida, D. A. (1987), On the variability of desert aerosol radiative characteristics, *J. Geophys. Res.*, *92*, 3017–3026.

Geleyn, J. F., and D. Tanré (1994), Short-term climatic response to the atmospheric aerosol radiative forcing, in *Passive Infrared Remote Sensing of Clouds and the Atmosphere II*, edited by D. K. Lynch, *Proc. SPIE*, *2309*, 243–246.

Hansen, J., M. Sato, and R. Ruedy (1997), Radiative forcing and climate response, *J. Geophys. Res.*, *102*, 6831–6864.

Haywood, J. M., R. P. Allan, I. Culverwell, T. Slingo, S. Milton, J. Edwards, and N. Clerbaux (2005), Can desert dust explain the outgoing longwave radiation anomaly over the Sahara during July 2003?, *J. Geophys. Res.*, *110*, D05105, doi:10.1029/2004JD005232.

Intergovernmental Panel on Climate Change (IPCC) (2001), *Climate Change 2001*, edited by J. Houghton, Cambridge Univ. Press, New York.

Janjic, Z. I. (1977), Pressure gradient force and advection scheme used for forecasting with steep and small scale topography, *Contr. Atmos. Phys.*, *50*, 186–199.

Janjic, Z. I. (1979), Forward-backward scheme modified to prevent two-grid-interval noise and its application in sigma coordinate models, *Contr. Atmos. Phys.*, *52*, 69–84.

Janjic, Z. I. (1984), Non-linear advection schemes and energy cascade on semi-staggered grids, *Mon. Weather Rev.*, *112*, 1234–1245.

Janjic, Z. I. (1990), The step-mountain coordinate: Physical package, *Mon. Weather Rev.*, *118*, 1429–1443.

Janjic, Z. I. (1994), The Step-mountain Eta Coordinate Model: Further developments of the convection, viscous sublayer and turbulence closure schemes, *Mon. Weather Rev.*, *122*, 927–945.

Janjic, Z. I. (1996a), The Mellor-Yamada Level 2.5 turbulence closure scheme in the NCEP Eta Model, in *Research Activities in Atmospheric and Oceanic Modelling*, *CAS/WGNE, 4.14–4.15*, World Meteorol. Org., Geneva.

Janjic, Z. I. (1996b), The surface layer parameterization in the NCEP Eta Model, in *Research Activities in Atmospheric and Oceanic Modelling*, *CAS/C WGNE, 4.16–4.17*, World Meteorol. Org., Geneva.

Janjic, Z. I. (2001), Nonsingular implementation of the Mellor-Yamada Level 2.5 scheme in the NCEP Meso model, *Office Note 437*, 61 pp. Natl. Cent. for Environ. Prediction, Camp Springs, Md. (Available at http://www.emc.ncep.noaa.gov/officenotes/FullTOC.html#2000)

Kaufman, Y. J., D. Tanré, O. Dubovik, A. Karnieli, and L. A. Remer (2001), Absorption of sunlight by dust as inferred from satellite and ground-based remote sensing, *Geophys. Res. Lett.*, *28*, 1479–1482.

Kaufman, Y. J., I. Koren, L. A. Remer, D. Rosenfeld, and Y. Rudich (2005), The effect of smoke, dust, and pollution aerosol on shallow cloud development over the Atlantic Ocean, *Proc. Natl. Acad. Sci. USA*, *102*(32), 11,207–11,212, doi:10.1073/pnas.0505191102.

Kischa, P., P. Alpert, J. Barkan, I. Kirchner, and B. Machenhauer (2003), Atmospheric response to Saharan dust deduced from ECMWF reanalysis (ERA) temperature increments, *Tellus, Ser. B*, *55*, 901–913.

Koepke, P., M. Hess, I. Schult, and E. P. Shettle (1997), Global aerosol data set, report, Max-Planck Inst. für Meteorol., Hamburg, Germany.

Lacis, A. A., and M. I. Mishchenko (1995), Climate forcing, climate sensitivity, and climate response: A radiative modeling persepctive on atmospheric aerosols, in *Aerosol Forcing of Climate: Report of the Dahlem Workshop on Aerosol Forcing of Climate, Berlin 1994, April 24–29*, edited by R. J. Charlson and J. Heintzenberg, John Wiley, Hoboken, N. J.

Levin, Z., E. Ganor, and V. Gladstein (1996), The effects of desert particles with sulfate on rain formation in the Eastern Mediterranenan, *J. Appl. Meteorol.*, *35*, 1511–1523.

Matthias, V., et al. (2004), Aerosol Lidar intercomparison in the framework of EARLINET project: 1. Instruments, *Appl. Opt.*, *43*, 961–976.

Mesinger, F., Z. I. Janjic, S. Nickovic, D. Gavrilov, and D. G. Deaven (1988), The step-mountain coordinate: model description and performance for cases of Alpine lee cyclogenesis and for a case of an Appalachian redevelopment, *Mon. Weather Rev.*, *116*, 1493–1518.

Miller, R. L., and I. Tegen (1998), Climate response to soil dust aerosols, *J. Clim.*, *11*, 3247–3267.

Miller, R. L., J. Perlwitz, and I. Tegen (2004a), Feedback upon dust emission by dust radiative forcing through the planetary boundary layer, *J. Geophys. Res.*, *109*, D24209, doi:10.1029/2004JD004912.

Miller, R. L., I. Tegen, and J. Perlwitz (2004b), Surface radiative forcing by soil dust aerosols and the hydrologic cycle, *J. Geophys. Res.*, *109*, D04203, doi:10.1029/2003JD004085.

Mishchenko, M. I., J. W. Hovenier, and L. D. Travis (2000), *Light Scattering by Nonspherical Particles*, 690 pp., Springer, New York.

Mishchenko, M. I., L. D. Travis, and A. A. Lacis (2002), *Scattering, Absorption, and Emission of Light by Small Particles*, Cambridge Univ. Press, Cambridge.

Myhre, G., A. Grini, J. M. Haywood, F. Stordal, B. Chatenet, D. Tanré, J. K. Sundet, K. Jostein, and I. S. A. Isaksen (2003), Modeling the radiative impact of mineral dust during the Saharan Dust Experiment (SHADE) campaign, *J. Geophys. Res.*, *108*(D18), 8579, doi:10.1029/2002JD002566.

Nickovic, S. (2005), Distribution of dust mass over particle sizes: Impacts on atmospheric optics, paper presented at Fourth ADEC Workshop: Aeolian Dust Experiment on Climate Impact, Ministry of the Environ., Nagasaki, Japan.

Nickovic, S., A. Papadopoulos, O. Kakaliagou, and G. Kallos (2001), Model for prediciton of desert dust cycle in the atmosphere, *J. Geophys. Res.*, *106*, 18,113–18,129.

Nickovic, S., G. Pejanovic, E. Ozsoy, C. Pérez, and J. M. Baldasano (2004), Interactive radiation-dust model: A step to further improve weather forecasts, paper presented at International Symposium on Sand and Dust Storm, World Meteorol. Org., Beijing, China.

Overpeck, J., D. Rind, A. Lacis, and R. Healy (1996), Possible role of dust-induced regional warming in abrupt climate-change during the last glacial period, *Nature*, *384*, 447–449.

Pérez, C., S. Nickovic, J. M. Baldasano, M. Sicard, F. Rocadenbosch, and V. E. Cachorro (2006), A long Saharan dust event over the western Mediterranean: Lidar, Sun photometer observations, and regional dust modeling, *J. Geophys. Res.*, doi:10.1029/2005JD006579, in press.

Perlwitz, J., I. Tegen, and R. L. Miller (2001), Interactive soil dust aerosol model in the GISS GCM: 1. Sensitivity of the soil dust cycle to radiative properties of soil dust aerosols, *J. Geophys. Res.*, *106*, 18,167–18,192.

Quijano, A. N., I. N. Sokolik, and O. B. Toon (2000), Radiative heating rates and direct radiative forcing by mineral dust in cloudy atmospheric conditions, *J. Geophys. Res.*, *105*, 12,207–12,219.

Rosenfeld, D., Y. Rudich, and R. Lahav (2001), Desert dust suppressing precipitation: A possible desertification feedback loop, *Proc. Natl. Acad. Sci. U.S.A.*, *98*, 5975–5980.

Rothman, L. S., et al. (1998), The HITRAN molecular spectroscopic database and HAWK (HITRAN Atmospheric Workstation): 1996 edition, *J. Quant. Spectrosc. Radiat. Transfer*, *60*, 665–710.

Schulz, M., Y. J. Balkanski, W. Guelle, and F. Dulac (1998), Role of aerosol size distribution and source location in a three-dimensional simulation of a Saharan dust episode tested against satellite-derived optical thickness, *J. Geophys. Res.*, *103*, 10,579–10,592.

Segal, M. (1990), On the impact of thermal stability on some rough flow effects over mobile surfaces, *Boundary Layer Meteorol.*, *52*, 193–198.

Shettle, E. P. (1984), Optical and radiative properties of a desert aerosol model, in *Proceedings of the Symposium on Radiation in the Atmosphere*, edited by G. Fiocco, pp. 74–77, A. Deepak, Hampton, Va.

Sokolik, I. N., and G. Golitsyn (1993), Investigation of optical and radiative properties of atmospheric dust aerosols, *Atmos., Environ., Ser. A*, *27*, 2509–2517.

Sokolik, I. N., and O. B Toon (1996), Direct radiative forcing by anthropogenic airborne mineral aerosols, *Nature*, *381*, 681–683.

Sokolik, I. N., and O. B Toon (1999), Incorporation of mineralogical composition into models of the radiative properties of mineral aerosolsfrom ultraviolet to infrared wavelengths, *J. Geophys. Res.*, *104*, 9423–9444.

Tegen, I., and A. A. Lacis (1996), Modeling of particle size distribution and its influence on the radiative properties of mineral dust aerosol, *J. Geophys. Res.*, *101*, 19,237–19,244.

Woodward, S. (2001), Modeling the atmospheric life cycle and radiative impact of mineral dust in the Hadley Centre climate model, *J. Geophys. Res.*, *106*, 18,155–18,166.

Yin, D., S. Nickovic, B. Barbaris, B. Chandy, and W. A. Sprigg (2005), Modeling wind-blown desert dust in the Southwestern United States for public health warning: A case study, *Atmos. Environ.*, *39*(33), 6243–6254.

Zhao, Q., and F. H. Carr (1997), A prognostic cloud scheme for operational NWP models, *Mon. Weather Rev.*, *125*, 1931–1953.

Zender, C. S., H. Bian, and D. Newman (2003), Mineral Dust Entrainment and Deposition (DEAD) model: Description and 990s dust climatology, *J. Geophys. Res.*, *108*(D14), 4416, doi:10.1029/2002JD002775.

J. M. Baldasano and C. Pérez, Earth Sciences Division, Barcelona Supercomputing Center, Edificio Nexus II, c/Jordi Girona 29, E-08034 Barcelona, Spain. (carlos.perez@bsc.es)

S. Nickovic, Environment Division, Atmospheric Research and Environment Program, World Meteorological Organization, 7 bis, Avenue de la Paix, BP2300, CH-1211 Geneva 2, Switzerland.

E. Özsoy, Institute of Marine Sciences, Middle East Technical University, P.k. 28, Erdemli-Mersin 33731, Turkey.

G. Pejanovic, South Environment and Weather Agency (SEWA), Zahumska 15, 11001 Belgrade, Serbia.